Chapter 4

STRONG ELECTRIC FIELD EFFECTS ON N-S_A AND S_A-N_R TRANSITIONS

4.1 Introduction

As described in Chapter 1 the smectic A (S_A) has a 1-dimensional translational order in addition to an orientational order of the nematic (N) phase [1, 2]. There are many systems which exhibit N-S_A phase transition (*eg* 8OCB). As the S_A phase has an additional **translational** order along the director A, it breaks the translational symmetry of the N phase along A. In view of the lower symmetry of the S_A phase, it usually occurs at lower temperatures compared to the N phase.

There are several theoretical models of the N-S_A phase transition. **McMillan** [47] has developed a molecular model of the N-S_A phase transition which is **an** extension of the Maier-Saupe [48] theory for the nematic-isotropic phase transition. This model predicts that the N-S_A transition can be either first order or second order depending on a parameter α (called the McMillan parameter) which is related to the chain length of the molecule. Following this argument by McMillan [47] de Gennes has developed a Landau theory [1] which also predicts that the N-S_A phase transition can be either first order or second order in nature. Here the order of the transition depends on a parameter which couples the orientational order and the smectic order. These models have been extended to include field effects on the N-S_A phase transition.

Rosenblatt [49] has used the Landau-de Gennes theory to study the effect of a strong magnetic field on a first order N-S_A phase transition. As the field is increased the transition temperature increases and at a critical field the nature of the N-S_A transition changes over from first order to **second** order. **McMillan's** molecular model has been extended by **Hama** [50] to study the effect of a magnetic field on a first order N-S_A phase transition to get similar results. Rosenblatt [39] has also studied the effect of a strong magnetic field on the S_A-Isotropic (S_A-I) transition. Using a lattice model previously developed by **himself** [51, 52], he predicted that a substantially large magnetic field **can** induce a *nonspontaneous* nematic phase in materials which exhibit only an S_A-I transition at zero field.

On the experimental side, to test the predictions of the models discussed in the previous paragraph, Lelidis and **Durand** [40] have studied the effect of a strong electric field on a system which undergoes a direct S_A-I phase transition. They used the technique **which** was described in Chapter 2, to measure the orientational order parameter as a function of field. They were able to observe a field induced first order phase transition from a paranematic phase to a nonspontaneous nematic phase. They were also able to obtain the critical field at which the first order phase transition becomes continuous, as in the case of the paranematic-spontaneous nematic phase transition described in Chapters 2 and 3. For higher values of the applied field they found

another first order phase transition from the nonspontaneous nematic phase to a phase with an orientational order parameter similar to that of the smectic A phase. They identified this to be a transition from the nematic to the smectic A phase.

As mentioned previously, in view of the lower symmetry of the S_A phase, it usually occurs at lower temperatures compared to the N phase. However, it is now well established that in compounds whose molecules have strongly polar cyano or nitro end groups, the nematic phase can reenter, as the S_A liquid crystal is cooled to a low enough temperature [5, 1, 2]. It is also established that the S_A phase which occurs between the higher temperature N phase and the lower temperature reentrant nematic (N_R) phase is characterised by a layer spacing d which is somewhat longer than the molecular length. This S_A phase with such a 'partial bilayer' structure is called the A_d phase and arises due to an antiparallel orientation between neighbouring polar molecules [16, 53] such that the aromatic cores overlap. Highly polar compounds also exhibit many other interesting phase sequences like double reentrance with a 'monolayer' smectic A_1 phase occurring at temperatures lower than the stability range of the N_R phase, smectic A polymorphism, occurrence of a reentrant nematic lake surrounded by the S_A phase in binary mixtures, etc [1]. All these phenomena have been successfully described by a Landau theory with two coupled smectic order parameters developed by **Prost** and co-workers [54]. The two order parameters correspond to the molecular length l and the length of the partial bilayer structure d (see Figure 4.1). Another simple way of describing the reentrant nematic phase is to construct a Landau theory in which the orientational and translational order parameters are appropriately coupled. As we mentioned earlier, following an argument of McMillan [47], de Gennes incorporated the lowest order coupling between the two order parameters which will enhance the bare S_A-N transition point [1]. A reentrant nematic phase can be obtained by introducing a higher order coupling which destabilises the smectic order when the orientational order is large [55]. Using such a model, the effect of an electric field (E) on the S_A-N_R transition has been worked out by Lelidis and Durand [55] who have shown that this transition point increases with E.

There have also been several attempts to develop molecular theories of the above phenomena. In particular, Berker and coworkers [56, 57] have developed a frustrated spin gas model in which triplets of polar molecules are considered to be the basic units and different internal configurations of these units give rise to the different phases mentioned above. In this model it is assumed that the orientational order is saturated in all the phases (S = 1).

The interaction between permanent dipoles favours an antiparallel orientation (A) between neighbouring molecules. This interaction energy is $\propto 1/r^3$ where r is the intermolecular separation. The strongest intermolecular interaction arises from the anisotropic dispersion energy between the aromatic cores resulting in the structure shown in Figure 4.1(a) which would give rise to a partial bilayer. If the polar molecules are parallel, the dipolar interaction is repulsive. However, in view of the strong polarisability of the conjugated aromatic core to which the dipole is attached, the latter induces an oppositely oriented dipole moment in the neighbouring molecule thus reducing the net dipole moment of each molecule (see Figure 4.1(b)). Further, in this 'parallel' or (P) configuration, the chains are in close proximity, adding to the attractive interaction. Both these effects are $\propto 1/r^6$. Hence, as the density is increased i.e. the temperature is lowered, one can expect a change in the configuration of the pairs from 'A' type to 'P' type. The two configurations shown in Figure 4.1 naturally account for the two length scales in the Landau theory developed by **Prost** [54]. The McMillan parameter which is a measure of the smectic interaction potential is larger for the 'A' type of pairs compared to that for the 'P' type of pairs. A molecular theory of double reentrance has been developed using these ideas
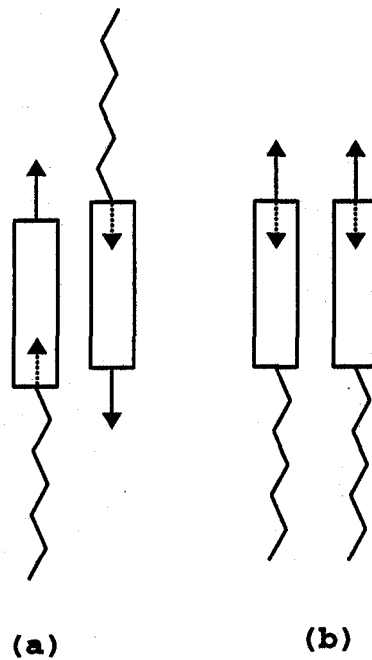
Figure 4.1: Schematic diagram showing the mutual configuration in an antiparallel 'A' (a) and a parallel 'P' (b) pair of polar molecules. The arrow head at the end of the solid line indicates the permanent dipole at the end of the molecule. The one with the dotted line is the dipole induced by the permanent dipole of the neighbouring molecule.

[58]. This model has been recently extended to account for other phenomena exhibited by polar compounds like nematic-nematic phase transition, smectic polymorphism, nematic lake e t $\neg_j$. [59, 60].

In this chapter we describe experimental results of the electric field effect on the N-A_d transition in 8OCB and on both the N-A_d and A_d-N_R transitions in an 8OCB-6OCB mixture which exhibits a reentrant nematic phase. Then we discuss the Landau-de Gennes theory of the N-S_A transition in the absence and in the presence of an external field. (We use the term S_A in the Landau theory in which the microscopic origin of the two lengths is not explicitly taken into account). We also discuss the effect of a strong electric field on the N-S_A and S_A-N_R phase transitions in the framework of an extended Landau-de Gennes theory. Finally we summarise the predictions of a molecular model developed by our coworkers, extended to include the electric field effect on the phase transitions in a system exhibiting a reentrant phase. [58, 59, 60].

4.2   Experimental

4.2.1   Strong Electric Field Effect on the N-A_d Phase Transition in 8OCB

The structure and transition temperatures of 8OCB are shown in Figure 4.2. The details of the experimental setup has been described in Chapter 2 and the block diagram is shown in Figure 2.19. We used a cell without the guard ring (Figure 2.2) and the top plate was aluminium coated (Figure 2.4). We used 19 μm spacers and have assumed that the thickness of the cell is equal to the thickness of the mylar spacer. At any given Mettler temperature, a few preset sinusoidal voltages were applied to the cell and at each voltage, the electrical parameters of the cell as well as its temperature were measured. All the measurements were made while cooling the sample
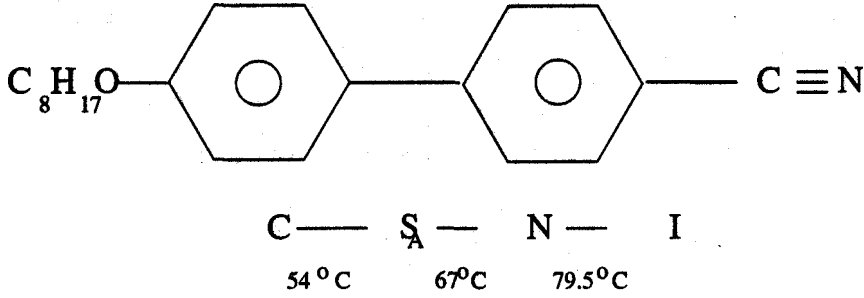
Figure 4.2: Structure and transition temperatures of 8OCB

from the nematic phase. A flow chart of the programme is shown in Figure 3.6. Figures 4.3 and 4.4 show the variation of the dielectric constant and the resistance of 8OCB across the N-S_A transition as a function of temperature at different fields.

The dielectric constant ($\epsilon_{\parallel}$) increases with field in both the nematic and the smectic A phase. The N-A_d phase transition is indicated by a slight decrease in $\epsilon_{\parallel}$ as the sample'is cooled. This is consistent with previous dielectric measurements on 8OCB [61]. The dielectric constant shows a relatively smooth variation across T_{AN} (the nematic-smectic A transition temperature) for higher fields and using this data it is difficult to locate the transition point clearly (see Figure 4.3). On the other hand, the resistance (R,) of the sample shows a negative jump as the sample is cooled across the transition temperature (Figure 4.4). This might seem unusual as the permeative process can be normally expected to decrease the mobility of ions along the layer normal in the smectic phase and hence to an increase in the resistance of the sample. However one should note that 8OCB has a partial bilayer structure and in such cases this effect is not very large [62].

On the other hand, $\epsilon_{\parallel}$ relaxes at a few MHz and even at $\sim$ 2000 Hz which is the frequency of measurement, there is a significant contribution of this relaxation to the effective conductivity of the sample. The total conductivity is given by

$$a(w) = \sigma(ion) + \frac{\epsilon_o \delta\epsilon_{\parallel}}{1 + \omega^2\tau^2}\tau\omega^2 \tag{4.1}$$

where τ is the relaxation time and $\delta\epsilon_{\parallel}$ is the difference in the dielectric constants corresponding to frequencies much lower and much higher than the relaxation frequency. The relaxation frequency of 8OCB close to T^*_{AN} (the field free transition temperature) is $\sim$ 6 MHz, and it further decreases sharply when the smectic order sets in [63]. The contributions of the relaxation to $\sigma(\omega)$ is $\sim$ 10 % at 2000 Hz and the negative jump in the resistance can be understood as arising from that in the relaxation frequency. As seen in Figure 4.4, in the nematic phase above $\sim$ 67°C the resistance of the sample increases with applied field. This effect in weak electrolytes is known as the phenomenon of limiting current [29] (to be discussed in Chapter 6). As the N-S_A transition is approached, the resistance decreases between E = 25.2 esu and E = 123.5 esu and increases at higher fields. This initial increase implies a slight misalignment of the sample in the smectic phase, which increases the effective resistance as $\sigma_{\parallel} > \sigma_{\perp}$ [62]. As the field is increased the alignment improves producing the normal trend above 123.5 esu. By identifying the temperature at which R, has a minimum as T^E_{AN} (the nematic-smectic A phase transition temperature in the presence of an electric field), we have plotted the latter as a function of the
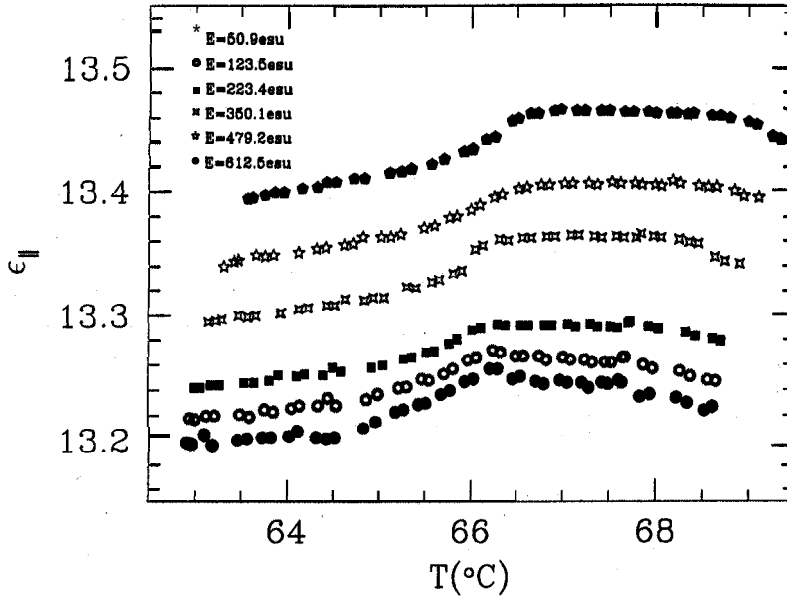
Figure **4.3:** Variation of the dielectric constant of 8OCB as a function of temperature for different electric fields across the N-S_A transition. $d = 19$ μm, $f = 2170$ Hz.
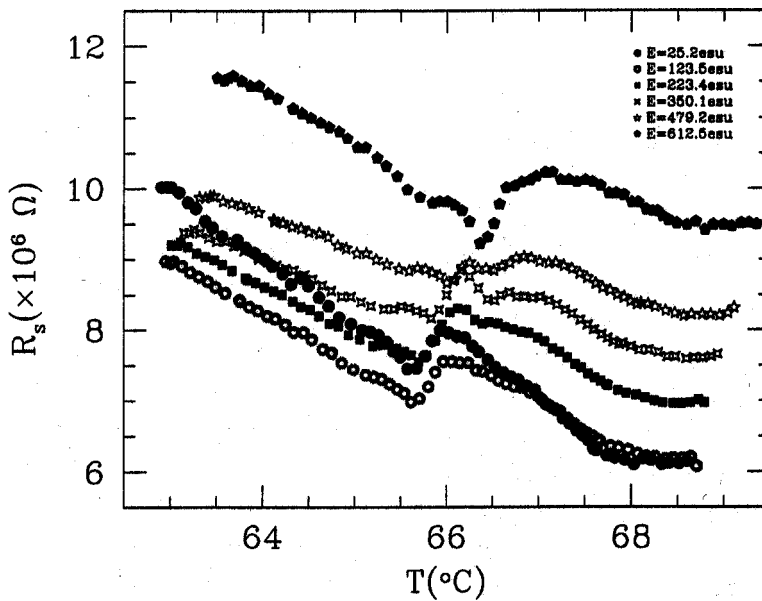

Figure 4.4: Variation of the resistance of 8OCB as a function of temperature at different electric fields across the N-S_A transition. $d = 19$ μm and $f = 2170$ Hz.
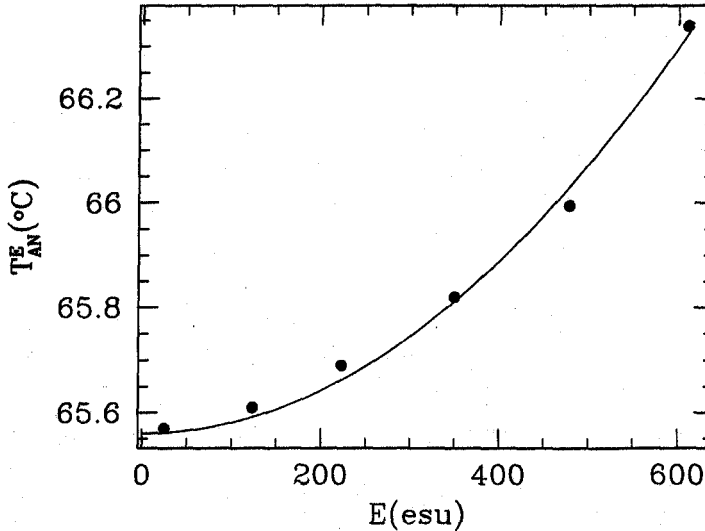
Figure 4.5: T_{AN}^E *as* a function of applied electric field in 8OCB. The symbols are experimental data taken from Figure 4.4. The calculated variation corresponds to $\gamma\chi/\alpha = -2.71 \times 10^{-5}$ cgs units (according to the Landau theory discussed in Section 4.3.1).

applied field in Figure 4.5. The data can be fitted quite well to a function of the form:

$$T_{AN}^E - T_{AN}^* \propto E^2. \tag{4.2}$$

This functional form can be derived using a Landau theory of the N-S_A transition (Section 4.3.1).

4.2.2 Field Effect on the N-A$_d$ and A$_d$-N$_R$ Transitions in an 8OCB-6OCB mixture

Mixtures of **hexyloxycyanobiphenyl** (**6OCB**) and **octyloxycyanobiphenyl** (**8OCB**) exhibit the phase sequence **isotropic-N-A$_d$-N$_R$** over a wide range of compositions. The molecular structures of the compounds and their transition temperatures are shown in Figures 4.2 and 4.6. Guillon et *al* [64] were the first to construct the phase diagram of the **8OCB-6OCB** mixture as a function of concentration (Figure 4.7).

As the N-A$_d$ and A$_d$-N$_R$ transitions occur at relatively low temperatures, mixtures of these compounds have been studied extensively [64, 66, 61, 65]. For our studies we have chosen a specific mixture with 27 wt % of **6OCB**. The pure compounds were obtained from Aldrich. The mixture has the following sequence of transitions: **Isotropic-78.3°C-N-47.2°C-A$_d$-28.4°C-N$_R$**. To study the effect of a strong electric field on the **8OCB-6OCB** mixture we have used both impedance measurements of the sample cell and a light scattering technique. The block diagrams of the light scattering and impedance analysis setups are shown in Figures 2.16, 2.14 and 2.13.
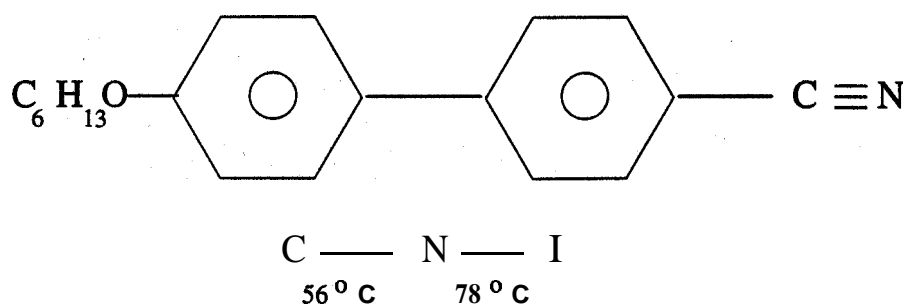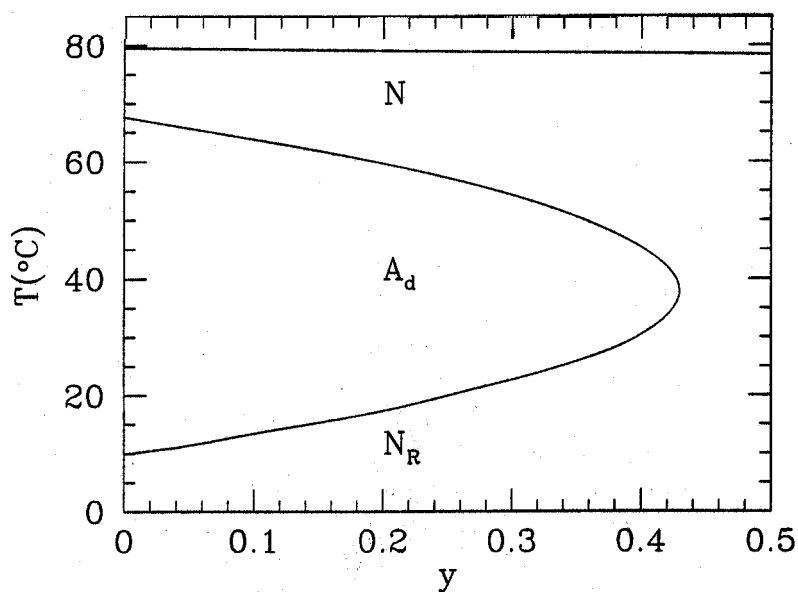
$$C_6H_{13}O - \text{phenyl} - \text{phenyl} - C \equiv N$$

$$C \underline{\quad\quad} N \underline{\quad\quad} I$$
$$56\,^{\circ}C \qquad 78\,^{\circ}C$$

Figure 4.6: Structure and transition temperatures of 6OCB

Figure 4.7: The phase diagram for 6OCB-8OCB mixture as a function of concentration. y is the molar ratio 6OCB:8OCB. (Taken from reference [65]).
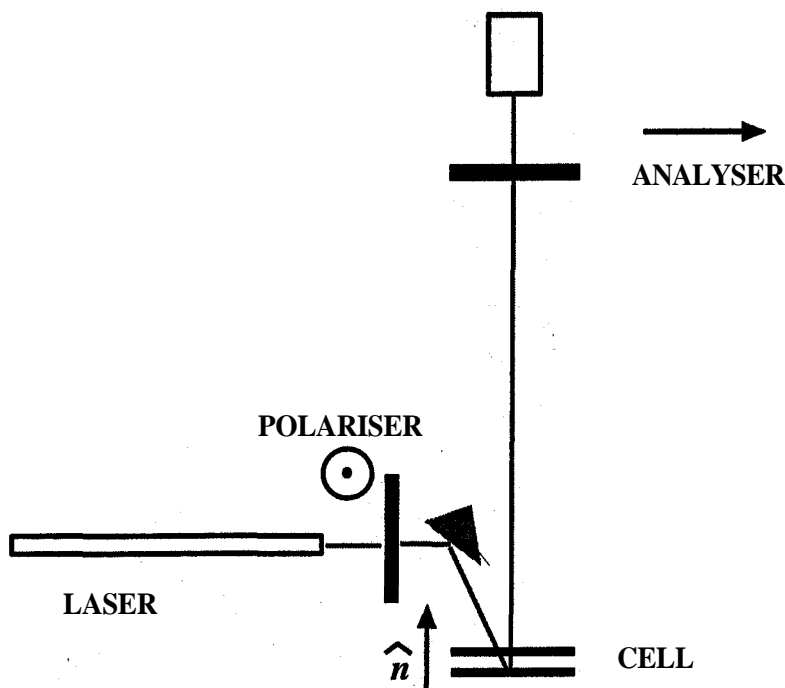
Figure 4.8: Scattering geometry used in the light scattering experiment. The angles are highly exaggerated for clarity.

4.2.2.1   Detection of the Nematic-Smectic A Phase Transition using the Light Scattering Technique.

Due to the thermal fluctuations of the director, the nematic liquid crystal strongly scatters light, thus leading to a turbid appearance for thick samples. It was shown by de Gennes [67] that for a given scattering angle the scattered intensity is inversely proportional to the Frank elastic constants of the medium.

$$I \propto \frac{\epsilon_{ai}^{z}}{K(T)} \tag{4.3}$$

where ϵ_{ai} is the anisotropy of the optical susceptibility and $K(T)$ is the angular average of the Frank constants defined by the scattering geometry. In our light scattering experiments a polarised He-Ne laser beam with its electric vibration normal to the plane of scattering, was chopped at 171 Hz and allowed to be incident on the sample through the upper transparent ITO electrode of the cell. The beam was reflected by the lower aluminium electrode. The reflected beam was cut off using an analyser and the back scattered light was collected using an INTEVAC intensified photo detector which has a relatively large cathode area. The output was monitored using a lock-in amplifier (Figure 2.16). The scattering geometry is shown in Figure 4.8. In this geometry the scattering is particularly strong for small scattering angles and we measure the scattered intensity due to twist fluctuations in the sample. In the smectic A phase twist fluctuations are not allowed and hence the twist elastic constant diverges as the nematic-smectic A phase transition point is approached. As seen from the Equation 4.3 this leads to a rapid fall in the scattered intensity as the sample is cooled across the nematic-smectic A phase transition. This has been used to detect [8] and study [68, 69] the N-S_A phase transition. Figure 4.9 shows the variation of the scattered light intensity over the nematic-smectic-reentrant nematic temperature range of the 6OCB-8OCB mixture.
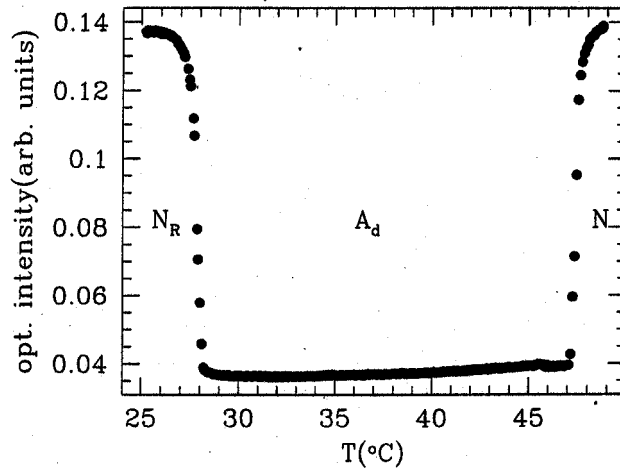
Figure **4.9:** Intensity of scattered light for $E = 0$ in the N-A_d-N_R temperature range for a homeotropically aligned sample of the 8OCB-6OCB mixture. Though 20 μm spacers were used the sample was not sealed Hence due to the larger thickness of the cell the scattered intensity varies sharply near the N-A_d and A_d-N_R transition points.

4.2.2.2 Experimental Procedure and Results

For these experiments we have used the improved cell and experimental setup (see Figures 2.3, **2.16** and 2.20). The lower plate of the cell included a guard ring, to reduce the edge effects, and the top plate was a transparent **ITO** coated plate, (Figure 2.4) to allow for light scattering measurements. Both the plates were treated with octadecyltriethoxysilane (ODSE) to get a homeotropic alignment of the liquid crystal. The sample thickness is typically $\sim$ 20 μm and has been measured just outside the periphery of the electrode by an interferometric technique described in Chapter **2.** As the interest was to study the effect of a large electric field on the phase transitions, it would have been advantageous to use thin cells ($\sim$ 10μm). But when we used cells of such thickness we saw that even in the nematic phase the fluctuations of the director were almost fully suppressed due to the surface effects. In such cases the N-A_d transition was not detectable even in the absence of an electric field. Hence we had to work with thicker cells ($\sim$ 20 μm). We have used a sinusoidal waveform to measure the variation of $\epsilon_{\parallel}$ and R_s in the N-A_d-N_R temperature range.

In the experiments described in Section **4.2.1** on 8OCB, at a constant set Mettler temperature the voltage is increased in steps. As mentioned previously the local heating of the sample depends on the applied voltage and the proximity of the temperature to the critical point of the sample (as seen in Figure 3.9 there is a large local heating around the critical region). Thus it is not possible to collect data at a constant temperature. The predictions of the theoretical models are usually shown as functions of temperature at different fields. To compare our experimental results to these theories it would be convenient if the experimental data are collected at a constant field as functions of temperature. To do this in the experiments to be described below we have adopted the following sequence. At a set applied voltage and frequency the temperature is decreased in steps (2°C). At each temperature **step** the data was collected after waiting for a few minutes for the temperature to stabilise. After the minimum temperature was obtained the run
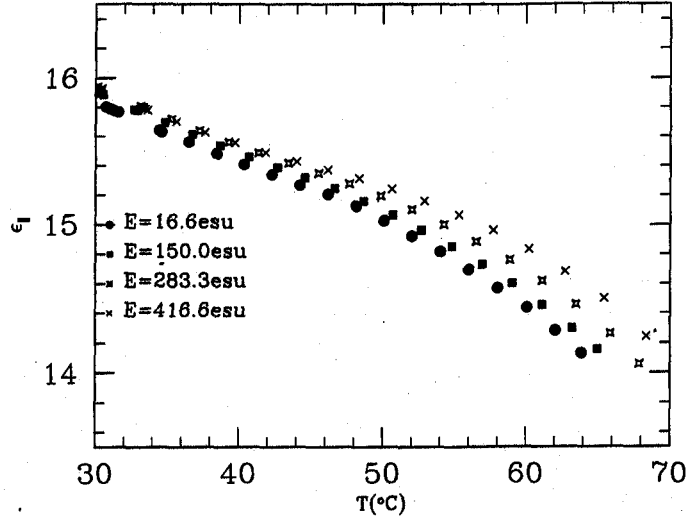
Figure 4.10: Variation of $\epsilon_\parallel$ for different fields in the N-A_d-N_R temperature range. $d = 20$ μm and f =4111 Hz.

was repeated for a different voltage. Figures 4.10 and 4.11 show the $\epsilon_\parallel$ and R_s measurements. We see from these figures that the quality (smoothness and continuity) of the data is better than that shown in Figures 4.3 and 4.4. This can be attributed to the better temperature control, inclusion of the guard ring and also the change in the experimental sequence.

As in the case of 8OCB (Section 4.2.1) as the field is increased the resistance of the sample increases in the present case also (Figure 4.11). This again can be attributed to the weak electrolytic nature of the sample thus leading to the limiting of the current. For the low field run $\epsilon_\parallel$ increases with decrease in temperature in agreement with previous measurements [61]. $\epsilon_\parallel$ increases with increase of electric field throughout the temperature range and it is seen that as the temperature is decreased, $\epsilon_\parallel$ increases by a smaller amount. Near the N-A_d transition region ($\sim 47°C$) there is a change of slope in both the $\epsilon_\parallel$ and R_s for all the fields. We also see a change of slope in both $\epsilon_\parallel$ and R_s around 30°C i.e. near the A_d-N_R phase transition point. Due to the large temperature step an accurate detection of the transition temperature is not attempted from these measurements.

To accurately detect the phase transition temperatures we have undertaken detailed electrical impedance and light scattering measurements across the phase transition regions. In some of these experimental runs also, we found it difficult to detect the N-A_d and A_d-N_R transitions using the electrical parameters of the cell as both $\epsilon_\parallel$ and the conductivity $\sigma_\parallel$ varied relatively smoothly across the transitions. Hence we used the simple light scattering technique described in the previous section to detect these transitions. We used a square wave voltage in these experiments.

The field free transition points (Figures 4.9 and 4.12) could be located only by the light scattering experiment. As the same lock-in amplifier was used for both light scattering and dielectric measurements, these runs were independent of each other. The temperature was lowered in steps of $\sim 0.08°C$ and the data were collected after waiting for a few minutes for stabilisation
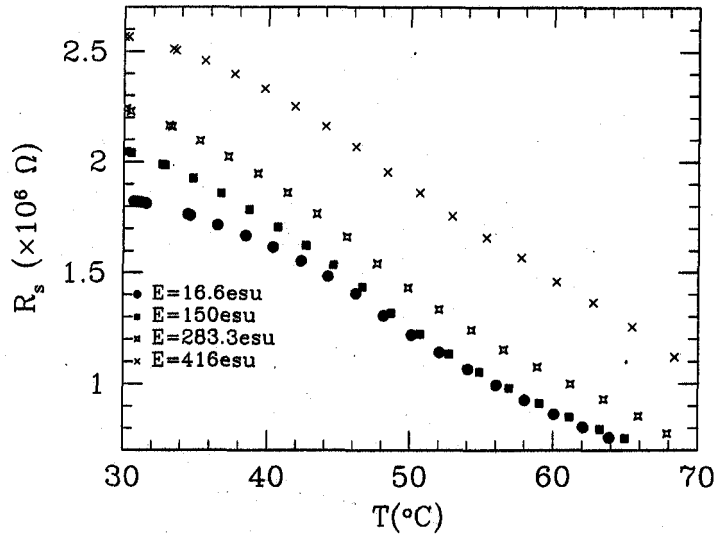
Figure 4.11: Variation of R_s for different fields in the N-A_d-N_R temperature range. $d = 20$ μm and $f = 4111$ Hz.

of temperature. A few representative runs of both the optical and dielectric measurements are shown in Figures 4.13 and 4.14.

As mentioned the temperature variation of the dielectric constant $\epsilon_{\parallel}$ in the N_R phase has a steeper slope compared to that in the A_d phase (Figure 4.14). We have used this fact to locate the A_d-N_R transition temperature in a few runs. In other runs the change in slope was not sharp enough to locate the transition temperature unequivocally using this technique.

As we have discussed in Section 4.2.1, in pure 8OCB, the N-A_d transition could be clearly detected because of a small but sharp decrease in R_s at the transition point. Though the permeation effect in the A_d phase could be expected to produce the opposite effect, as we argued, the sharp decrease in the relaxation frequency of $\epsilon_{\parallel}$ which contributes to the conductivity even at the frequency of measurement, would lead to the observed trend. Figure 4.14 shows the temperature variation of resistance in the reentrant mixture at 333.3 esu. The dip in R_s is clearly seen at the N-A_d transition temperature. On the other hand, there is only a small change of slope at the A_d-N_R transition temperature. As in the case of the dielectric data the resistance measurements were used to locate the transition temperature in those cases in which the signature was unambiguous. We found that the temperatures agreed with the optical measurements to about $\pm$ 0.5°C for the A_d-N_R transition point. As all the experiments are conducted while cooling the sample the scatter in the data may partly arise from different extents of supercooling. The agreement between the two independent types of measurements is better for the N-A_d transition ($\sim \pm 0.2$°C). The field free N_R - A_d and A_d-N transition points were checked before the start of the experiment, and after it was completed, and were found to be constant to within $\pm$ 0.2°C, which is less than the uncertainty in locating the A_d-N_R transition temperature using different techniques.

Both the A_d-N_R and A_d-N transition temperatures increase with field though the variation of the former is much stronger than that of the latter. We have applied fields up to 500 esu (at
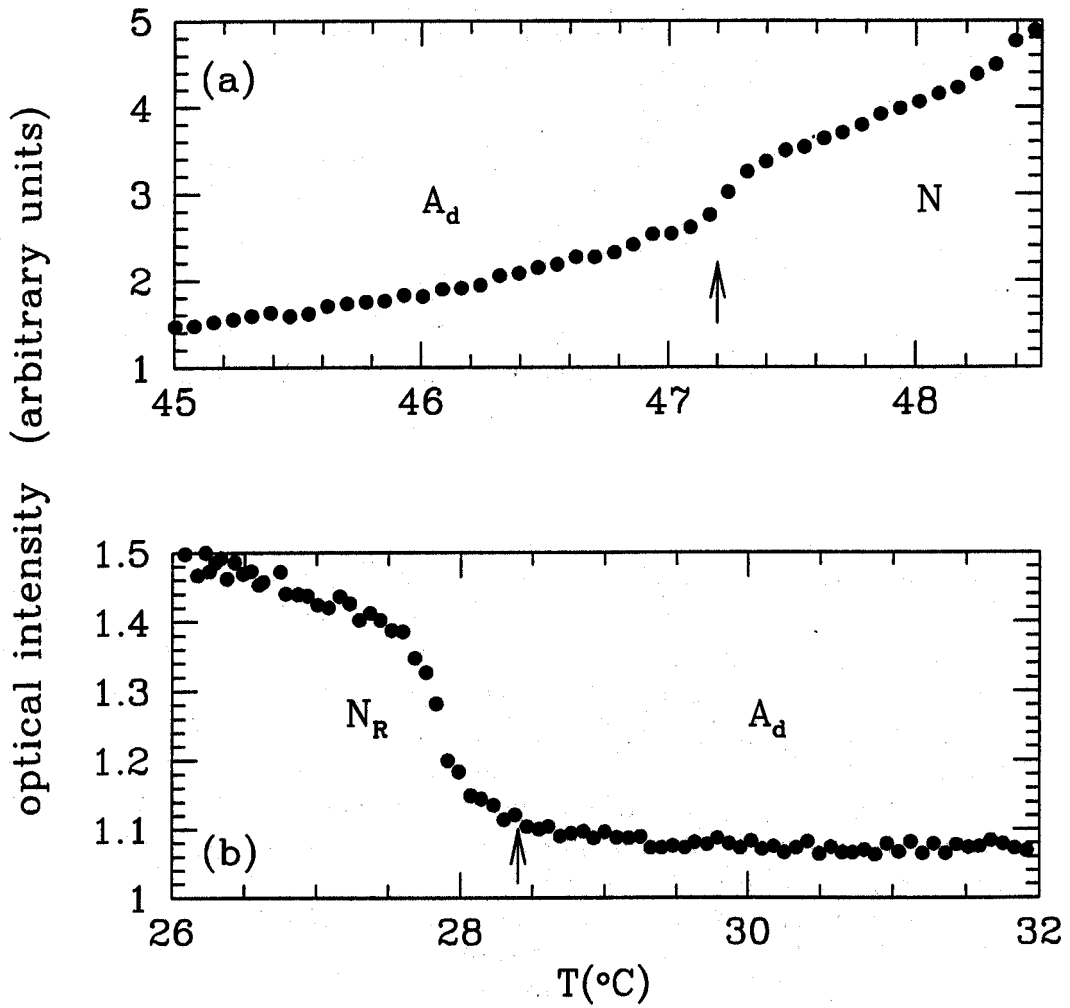
Figure 4.12: Intensity of scattered light as a function of temperature for $E = 0$ (a) near the A_d-N transition point and (b) near the A_d-N_R transition point. The transition temperatures are indicated by arrows. Here the sample **was** sealed and the thickness was measured to be 20 μm. The scattered intensity varies less sharply than shown in Figure 4.9 due to the smaller thickness.
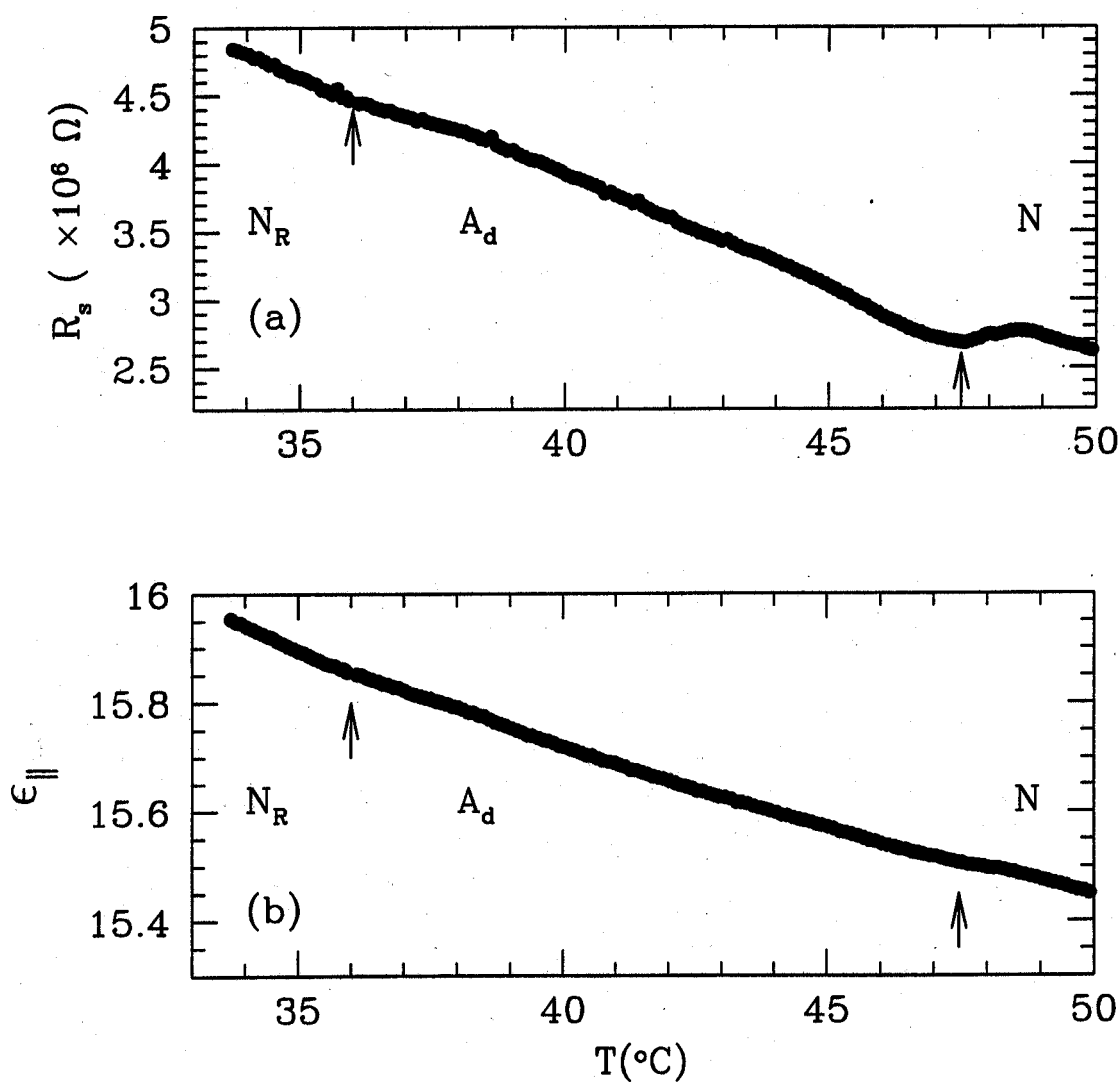
Figure **4.14:** (a) Resistance of the cell at **333.3** esu as a function of temperature. The arrows indicate A_d-N_R and A_d- N transition points. Thickness of the cell is $\sim$ **20** μm and the frequency of the applied voltage is **4111** Hz. (b) Dielectric constant of the cell at **333.33** esu as a function of temperature. The arrows are drawn at the same positions as in (a).
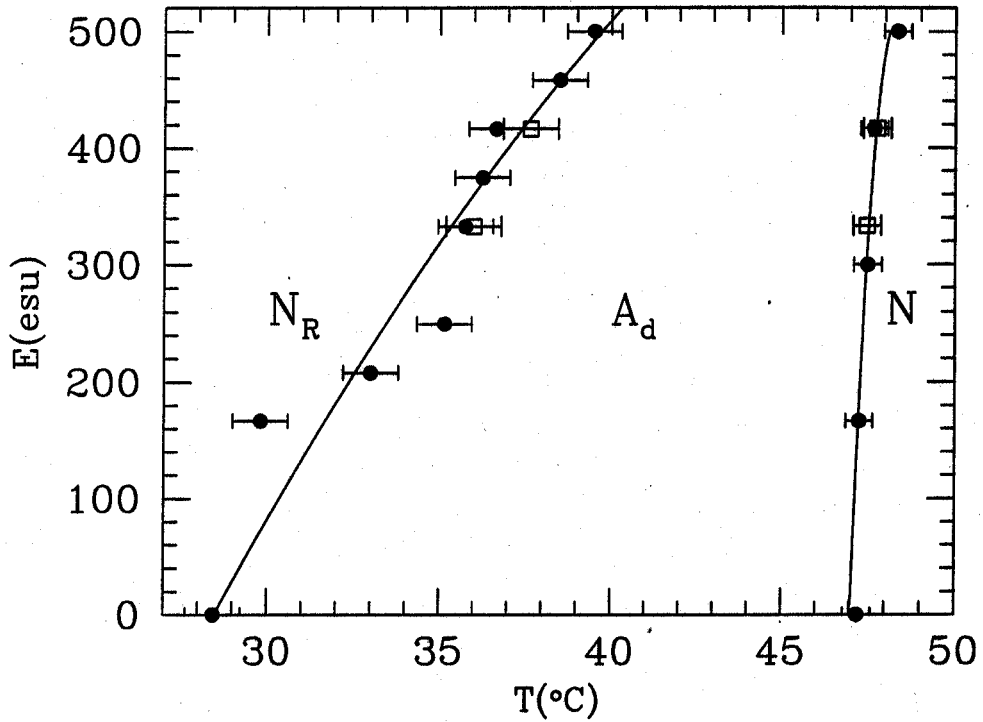
Figure **4.15:** The electric field phase diagram for the 60CB ‑ 80CB mixture. Circles are data obtained from light scattering measurements and open squares are those obtained from the electrical impedance measurements. The solid lines are guides to the eye. Note that the data on the N_R-A_d transition are consistent with a change of slope at **200** esu.

4111 Hz) on a sample with thickness $\sim$ **20** μm to construct the phase diagram shown in Figure **4.15.** Though we have shown the field dependence of the A_d-N_R transition temperature by a smooth line as a guide to the eye note that the data is consistent with a change of slope at $\sim$ **200** esu. In Sections **4.3.2** and **4.3.3** we describe some theoretical models which describe this electric field phase diagram.

4.3   Theoretical Interpretation

4.3.1   Landau Theory for the N-S_A Transition

As described previously the smectic **A** phase is characterised by a density modulation in a direction $\vec{z}$ orthogonal to the layers:

$$\psi(z) = \psi_1 \cos(q_o z + \phi) + \dots \tag{4.4}$$

where ψ_1 is the amplitude of the first harmonic of the density modulation, q_o is the wave vector of the modulation and ϕ an arbitrary phase. In nematics $\psi_1 = 0$. Thus ψ_1 is a natural order parameter for the S_A phase. The S_A order parameter can be specified by the complex quantity

$$\psi = |\psi| e^{i\phi}. \tag{4.5}$$

de Gennes described the N-S_A phase transition on the basis of a Landau theory. In the vicinity of the N-S_A transition the free energy density can be expanded in powers of $|\psi|$

$$f_s = \frac{1}{2} A_A |\psi|^2 + \frac{1}{4} C_A |\psi|^4 + \dots \tag{4.6}$$

Only even powers of ψ are needed since $\pm\psi$ differ only in the origin of the reference' axis. $A_A = a_A(T - T_{AN}^*)$ and C_A are the usual Landau coefficients. This can give a second order phase transition at $T = T_{AN}^*$ if $C_A > 0$.

The orientational order couples with the translational order and enhances the orientational order parameter **S** which can be written as

$$S = S_o + \delta S \tag{4.7}$$

where S_o is the excess orientational order in the absence of the smectic order. The coupling of the translational order to the orientational order to the lowest order must have the form

$$f_1 = \gamma |\psi|^2 \delta S \tag{4.8}$$

where γ is a negative constant. Including the nematic free energy which has a minimum for $\delta S = 0$

$$F_N = F_N(S_o) + \frac{1}{2|\chi|} \delta S^2 \tag{4.9}$$

where χ is a response function which is large near the N-I phase transition point T_{NI}, but is small for $\mathbf{T} \ll T_{NI}$. The overall free energy F_S is obtained by adding f_s, f_1 and F_N

$$\begin{aligned} F_S &= \frac{a_A(T - T_{AN}^*)}{2} |\psi|^2 + \frac{C_A}{4} |\psi|^4 + \gamma |\psi|^2 (S - S_o) \\ &+ \frac{(S - S_o)^2}{2\chi} + F_N(S_o). \end{aligned} \tag{4.10}$$

As was argued by de Gennes [1], when χ is small i.e. if the nematic range is large ($\sim 10°C$), the S_A-N transition remains second order in nature. In our experiments we have studied 8OCB which has a large nematic range (12.5°C) thus we can assume that χ is small. Also calorimetric measurements on 8OCB suggest that the N-S_A phase transition in 8OCB is second order in nature [70].

4.3.1.1 Landau Theory for the S_A-N Transition in the Presence of an Electric Field

Adding the electric field dependence to the free energy density in the model described in the previous section, we get

$$F_S^E = \frac{a_A(T - T_{AN}^*)}{2}|\psi|^2 + \frac{C_A}{4}|\psi|^4 + \gamma|\psi|^2(S - S_o)$$
$$+ \frac{(S - S_o)^2}{2\chi} + F_N(S_o) - \frac{\Delta\epsilon_o}{12\pi}E^2 S. \tag{4.11}$$

Minimising the above free energy with respect to S we get

$$S = S_o - \chi\gamma|\psi|^2 + \frac{\chi\Delta\epsilon_o}{12\pi}E^2. \tag{4.12}$$

and substituting this value in Equation 4.11, we get

$$F_S^E = \frac{a_A}{2}\left\{T - \left(T_{AN}^* - \frac{\gamma\chi\Delta\epsilon_o}{6\alpha\pi}E^2\right)\right\}|\psi|^2 + \left(\frac{C_A}{4} + \gamma\chi^2/2\right)|\psi|^4 \tag{4.13}$$

The above equation leads to an enhancement of T_{AN}^* (as γ is negative) which is quadratic in the electric field. We have fitted the experimental data shown in Figure 4.5 to the form $T_{AN}^E = T_{AN}^* - \frac{\gamma\chi\Delta\epsilon_o}{6\alpha\pi}E^2$. This yields $\frac{\gamma\chi}{\alpha} = -2.71 \times 10^{-5}$ cgs units for 8OCB.

4.3.2 Landau Theory for the Electric Field Phase Diagram for Systems Exhibiting Reentrant Phases

As we mentioned in the introduction of this chapter, Lelidis and Durand [55] have used a coupling of the type $|\psi|^2 (\gamma S + \Lambda S^2/2)$ between the smectic ($|\psi|$) and nematic (S) order parameters in the Landau free energy density to obtain the S_A-N_R transition. Note that the coupling term is now taken to be of the form $\gamma S|\psi|^2$ instead of $\gamma\delta S|\psi|^2$ in Equation 4.11 which will yield the same results as S_o is a constant. The calculations show that the S_A-N_R transition point increases with the applied electric field, as the field induced enhancement in the orientational order destabilises the smectic phase due to the positive sign of A.

In our experimental system we have both N-S_A and S_A-N_R transitions. We extend the Landau model by introducing a higher order coupling between the smectic and nematic order parameters to get both the transitions. As there are several compounds which exhibit a reentrant smectic phase below the range of the N_R phase we include a higher order coupling term which is cubic in S. The free energy density is now written as:

$$F_S^E = F_N(S_o) + \frac{(S - S_o)^2}{2\chi} + \mu_e E^2 S + \frac{A_A}{2}|\psi|^2 + \frac{C_A}{4}|\psi|^4$$
$$+ \left(\gamma S + \frac{\Lambda}{2}S^2 + \frac{\delta}{3}S^3\right)|\psi|^2. \tag{4.14}$$

The coupling between the orientational order parameter is now given by the last term. $\mu_e = -\Delta\epsilon_o/(12\pi)$, where $\Delta\epsilon_o$ is the dielectric anisotropy of the nematic with S =1. Minimising Equation 4.14 with respect to S we get

$$S = \left\{-(\chi\Lambda|\psi|^2 + 1) \pm [(\chi\Lambda|\psi|^2 + 1)^2\right.$$
$$\left. -4\chi\delta|\psi|^2(\chi\mu_e E^2 + \chi\gamma|\psi|^2 - S_o)]^{1/2}\right\}/$$
$$(2\chi\delta|\psi|^2). \tag{4.15}$$

As we are interested only in locating the second order S_A-N transition points near which $|\psi|^2$ is very small, we can expand the terms in the square root and neglect higher order terms to obtain

$$S \simeq (S_o - \chi\mu_e E^2) + \frac{\chi|\psi|^2}{4}\{-4(\gamma + S_o^2\delta) - 4\Lambda(S_o - \chi\mu_e E^2)$$
$$+ \ 4\chi\mu_e E^2\delta(2S_o - \chi\mu_e E^2)\} \tag{4.16}$$

where we have used only the positive sign in Equation 4.15 as the other sign leads to unphysical results. Substituting this in Equation 4.14 and collecting the terms which depend on $|\psi|^2$ we find that the latter has the form

$$|\psi|^2\frac{a_A}{2}\left[T - \left\{T_{AN}^* - \frac{2\gamma}{a_A}\left(S_o - \chi\mu_e E^2\right) - \frac{\Lambda}{a_A}\left(S_o - \chi\mu_e E^2\right)^2 - \frac{2}{3}\frac{\delta}{a_A}\left(S_o - \chi\mu_e E^2\right)^3\right\}\right] \tag{4.17}$$

in which $S(E) = S_o - \chi\mu_e E^2$ is the field enhanced orientational order parameter. It is clear that the coupling between the translational and orientational orders, and the enhancement of the orientational order due to the field both contribute to a shift in the A-N transition point from the bare value T_{AN}^*. At the renormalised transition temperature the above term goes to zero and the smectic phase is stable when it is negative. In order to calculate the phase diagram it is necessary to know both S_o the nematic order parameter, and the field enhanced value $S(E)$. One could have used a Landau theory of the weakly first order nematic-isotropic phase transition for calculating S_o [55]. Near the transition temperature, this would lead to $S_o \sim \left((T^\dagger - T)/T^\dagger\right)^\beta$ with $\beta = 0.5$ where $T^\dagger$ is a temperature which is slightly above the first order N-I transition point T_{NI}. However experimental data on a number of compounds can be fitted only if the index β is much lower, ~ 0.25 [1]. Both the N-S_A and S_A-N_R transitions occur well below T_{NI} in the system used by us, and we have used $\beta = 0.25$ to calculate S_o at various temperatures. The susceptibility χ also should depend on S_o, decreasing as S_o increases. As we are interested only in the S_A-N_R and S_A-N transition points both of which occur at temperatures well below T_{NI}, for simplicity we have assumed that χ is constant over the temperature interval of interest. We have used the following parameters in our calculations: $T_{AN}^* = 325$ K, $T^\dagger = 350$ K, $\beta = 0.25$, 2 $\gamma/a_A = -45.9$, $\Lambda/a_A = -183.9$, $2\delta/3a_A = 528$ and $\mu_e\chi = -1.6 \times 10^{-9}$. In the field free case, the above model leads to the following transitions: N-S_A at 320.5 K and S_A-N_R at 298.8 K which roughly correspond to the transition temperatures in the experimental system. Interestingly, the model predicts a reentrant smectic phase also i.e. an N_R to S_{AR} transition at 279.2 K. Though many compounds are now known to exhibit a reentrant smectic A phase (which has a monolayer spacing) [1] the system that we have studied crystallises well above this possible transition, and we will not discuss the reentrant smectic phase any further. The calculated phase diagram in the range of experimental interest is shown in Figure 4.16. The S_A-N_R transition temperature shows a large increase with field as found in the experiment. However, the calculated N-S_A transition temperature slightly decreases with field unlike in the experimental case, and the S_A phase is bounded. The destabilisation of the smectic phase occurs essentially because of the highest order coupling of the orientational and translational orders which increases with field. In the phenomenological Landau model the origin of the different signs of the coefficients is not clew. The physical origin of the destabilisation of the S_A phase is of course of fundamental interest. In the next section we will discuss a molecular theory of highly polar compounds for this purpose.
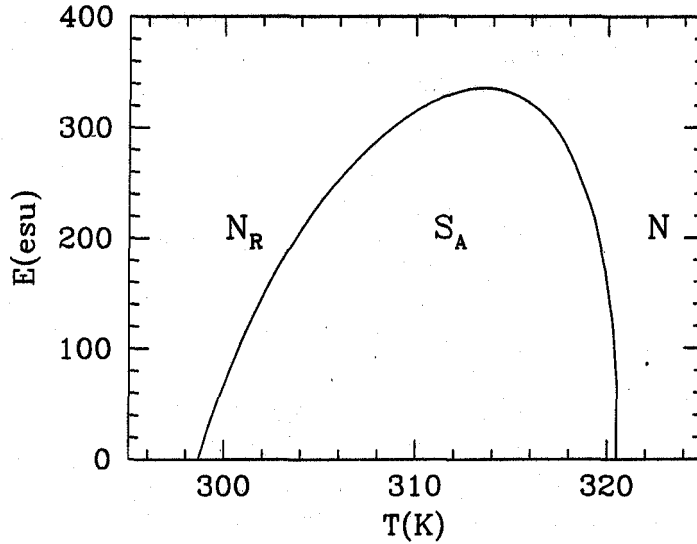
Figure 4.16: The electric field phase diagram calculated on the basis of the Landau theory presented in the text.

4.3.3 Molecular Model for the Electric Field Phase Diagram of a Mixture Exhibiting the Reentrant Nematic Phase

In this section we briefly describe a molecular model developed by our coworkers [58, 59, 60] and extended to describe the electric field effect on the phase transition in a system which exhibits reentrant nematic phase. As described in the introduction of this chapter the medium is assumed to consist of 'pairs' of molecules having either antiparallel (A) or parallel (P) configurations (Figure 4.1). Frustration in the orientation of a third molecule can lead to stable pairs with A-type of configuration. On the other hand, a large number of molecules can be associated in the P-type configuration. It has been assumed that even the P-type configuration consists of only pairs.

As described earlier, the A-type (P-type) configuration is favoured at lower (higher) densities. Again, for the sake of simplicity, it has been assumed that the energy difference between the two configurations has the following form:

$$\Delta \mathcal{E} = \mathcal{E}_A - \mathcal{E}_P = \mathcal{R}_1 k_B T_{NI} \left(\frac{\mathcal{R}_2}{T_R} - 1 \right) \tag{4.18}$$

where k_B is the Boltzmann constant, $\mathcal{E}_A$ and $\mathcal{E}_P$ are the configurational energies of the A-type and P-type pairs respectively, T_{NI} is the nematic-isotropic transition temperature of the A-type of pairs, $\mathcal{R}_1 k_B T_{NI}$ is an interaction parameter and $T_R = T/T_{NI}$ is the reduced temperature. $\mathcal{R}_2$ is the reduced temperature at which the density of the medium is such that $\Delta \mathcal{E}$ becomes zero. For $T_R > \mathcal{R}_2$, the A-type configuration has the lower energy. $\mathcal{R}_2$ can be expected to depend weakly on the chain length in a homologous series i.e. on the McMillan parameter a. The dependence of $\mathcal{R}_2$ on a is ignored.

The electric field can in general be expected to enhance the density of the medium (elec-

trostriction). The 'direct' effect arises from the pressure due to the field, $\kappa_E = \epsilon_\parallel E^2/(8\pi)$ and yields $\delta\rho/\rho = \kappa_T \epsilon_\parallel E^2/(8\pi)$, where κ_T is the isothermal compressibility. For the highest field that has been applied , $\delta\rho/\rho \sim 10^{-5}$. However, as **was** mentioned, the anisotropy of dielectric constant couples to the field to enhance the order parameter of the medium. This results in another contribution to the electrostriction.

$$\delta\rho = \left[\frac{\partial\rho}{\partial S}\right]_T \delta S(E) \tag{4.19}$$

with

$$\delta S(E) = \frac{\chi\Delta\epsilon_o E^2}{12\pi} \tag{4.20}$$

where χ is the susceptibility for the orientational order and has been assumed to be $\sim 4\times10^{-8}$ in the calculations. Horn [71] has measured the order parameter of pentyl cyanobiphenyl as a function of pressure and at temperatures much lower than T_{NI}, $[\partial\rho/\partial S]_T$, $\simeq 0.3$. Using these values, $\delta\rho/\rho$ at the highest fields used $\sim 2 \times 10^{-3}$, which is 200 times larger than the direct electrostriction effect estimated earlier. Hence the intermolecular separation decreases with E^2, and this can in turn be expected to change $\mathcal{R}_2$. In view of the above discussions, it can be written that

$$\mathcal{R}_2(E) = \mathcal{R}_2(0) + CE^2. \tag{4.21}$$

C is estimated from earlier [58] calculation of the variation of AE given by Equation 4.18 with r the intermolecular separation and is found to be $\simeq 10^{-8}$ cgs units. Our dielectric measurements on the 60CB-80CB mixture used in the experiment reported in Section 4.2.2.2 (Figure 4.10) clearly indicate that the susceptibility χ has a value $\simeq 3 \times 10^{-7}$ near the N_R -A transition temperature. The larger value shows that the concentration of parallel pairs is relatively high in this mixture, compared to that in 5CB, as it should be for the occurrence of the reentrant nematic phase. Indeed in another compound which shows only a nematic phase but with a relatively large fraction of parallel pairs, χ has a similarly large value (see the next chapter). It is assumed that $C = 8\times 10^{-8}$cgs units in Equation 4.21. The possible volume-dependence of the orientational and layering potentials has not been taken into account, the affect of which will be much smaller than the one discussed above.

In order to calculate the enhancement due to the field in the orientational order parameter in the context of a molecular model, it is necessary to use the orienting effect of the field on the dipole moments as well as the anisotropic polarisabilities of the molecules. For the sake of simplicity, it is assumed that due to the field both the A and P type pairs have an orienting potential of the form,

$$U_A(E) = -\beta_A E^2 \cos^2\theta_A$$

and

$$U_P(E) = -\beta_P E^2 \cos^2\theta_P \tag{4.22}$$

where β_A and β_P can be estimated from the known dielectric anisotropy. We get $\beta_A \simeq 1000/N_A$ cgs units where N_A is the Avogadro number. It is known from dielectric studies [61] that the dielectric anisotropy for the N_R phase in which the P-type of pairs dominate is $\sim 10\,\%$ higher
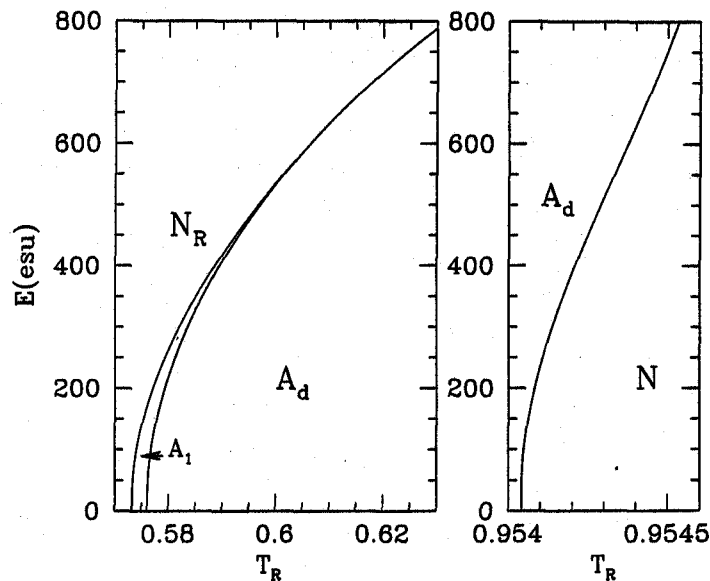
Figure **4.17:** Calculated phase diagram showing the smectic-smectic line meeting the N_R-A_d line at $E \sim 600$ esu and $T_R \simeq 0.607$.

than that for the A_d-phase in which the **A** type pairs dominate. As such, $\beta_P \simeq 1.1 \, \beta_A$ has been used.

Using these ingredients and a suitable extension of the Mcmillan theory of smectic A phase the mixtures of the two types of pairs, calculations have been made for an appropriate set of parameters.

The calculations yield the phase diagram shown in Figure **4.17.** Both the A_d-N and the smectic-N_R phase transitions increase with temperature. For lower values of the electric field there is a A_1-N_R phase transition. As the field is increased, the A_d-A_1 and A_1-N_R lines meet at higher fields and only the A_d-N_R transition is realised. The change of slope of the smectic to N_R transition line is similar to that seen in the experimental diagram (Figure **4.15).** The A_d-A_1 transition temperature is well separated from the smectic to N_R transition when $E = 0$. Xray studies on the mixture used in our experiments have been conducted [66]. However, they are not accurate enough to have detected a smectic A to smectic A transition.

It can be seen from the experimental phase diagram that as the electric field is increased the temperature range of the A_d phase decreases (Figure **4.15).** This indicates that for a field higher than the maximum field used in the experiment ($E = 500$ esu) the A_d phase may get bounded above. This is reminiscent of the pressure temperature phase **diagram** seen in mixtures exhibiting reentrant nematic **phases** [72]. For the concentration of the 8OCB-6OCB mixture which we have used we have not been able to attain this field. The qualitative agreement between the experimental (Figure **4.15)** and theoretical phase diagrams (Figure **4.17)** supports the assumption that the medium consists of a mixture of **molecules** having both parallel and antiparallel configurations. The parallel configuration is favoured at lower temperatures (higher densities). The effective dipole moment of the parallel configuration is larger than that of the antiparallel **configuration.** The above arguments imply that at lower temperatures there are polar short range ordered groups in the medium whose concentration increases **as** the temperature is

lowered. This could be verified if xray studies on this mixture are conducted in the presence of a strong electric field.

In the next chapter we present experimental results on a highly polar nematogen. Indeed from these results we find further evidence for polar short range order.